Partially coherent twisted states in arrays of coupled phase oscillators

Oleh E. Omel'chenko and Matthias Wolfrum

Weierstrass Institute, Mohrenstrasse 39, 10117 Berlin, Germany

Carlo R. Laing

INMS, Massey University, Private Bag 102-904 NSMC, Auckland, New Zealand

We consider a one-dimensional array of phase oscillators with non-local coupling and a Lorenztian distribution of natural frequencies. The primary objects of interest are partially coherent states that are uniformly "twisted" in space. To analyze these we take the continuum limit, perform an Ott/Antonsen reduction, integrate over the natural frequencies and study the resulting spatio-temporal system on an unbounded domain. We show that these twisted states and their stability can be calculated explicitly. We find that stable twisted states with different wave numbers appear for increasing coupling strength in the well-known Eckhaus scenario. Simulations of finite arrays of oscillators show good agreement with results of the analysis of the infinite system.

The classical results of Kuramoto describe the transition from disordered (incoherent) to synchronized (coherent) behavior in a population of globally coupled oscillators with randomly chosen inhomogeneous frequencies: Increasing the coupling strength, there is a threshold where the incoherent state loses its stability and a stable branch of partially coherent states with an increasing fraction of the oscillators being synchronized appears. It is a fundamental question, how this scenario extends to various types of spatially extended systems. For the simple case of a one-dimensional array with non-local coupling and identical oscillators there appear uniformly twisted states, in which the phase increases linearly with distance along the array. Their existence and stability was analyzed in [**27**]. Here we consider similar solutions that occur in networks of *nonidentical* phase oscillators, each having a different intrinsic frequency. These solutions are described by a spatially-dependent complex order parameter, and the argument of this is identified with the phase of a partially coherent twisted state. We derive an equation governing the evolution of this order parameter in the continuum limit and show that it can be reduced to a simpler equation using the Ott/Antonsen ansatz. Partially coherent twisted states are described exactly, and their stability calculated analytically. We find that for increasing coupling strength twisted states with different twists (wave numbers) appear gradually in a scenario that resembles the classical Eckhaus instability describing the emergence of stable wave patterns in partial differential equations. Finally, we verify our results using simulations of finite networks of oscillators.

I. INTRODUCTION

Coupled oscillator networks have been studied for many years as models of a variety of natural and man-made phenomena [20]. One useful simplification in their study, valid when oscillators are weakly coupled, is to describe the state of each oscillator by a single angular variable, its phase. In the simplest case, the interaction of the oscillators is described by sinusoidal functions of their phase differences [2, 3, 19, 24]. Over the last decade a number of researchers have considered spatially-extended networks of phase oscillators, coupled nonlocally [7, 9, 10, 14, 22, 23]. Several interesting phenomena have been studied in such systems, including "chimera" states, which show regions of synchrony alternating with asynchronous regions [1, 8, 11], and uniformly twisted states, in which the phase difference between neighboring (identical) oscillators is fixed [6, 21, 27].

All of these studies of twisted waves have considered *identical* oscillators, coupled in a highly-symmetric fashion (although see [12] for a network with partially-random coupling). However, in reality no system is ever perfect and it is of interest to consider the effects of heterogeneity on the types of dynamics seen in highly-symmetric systems. In this paper we analyze the effects of heterogeneity (in the form of non-identical intrinsic frequencies) on the existence and stability of twisted waves seen in arrays of non-locally coupled phase oscillators. Because of the heterogeneity, there appear twisted states that are only partially coherent. Due to heterogeneity, their twist can no longer be defined by a constant phase difference between neighboring oscillators. Instead, we use the twist of a complex local mean field, given at each point in the array via a sum or integral over oscillator phases in a certain neighborhood.

Our basic model is an array of non-locally coupled phase oscillators

$$\frac{d\theta_k}{dt} = \omega_k - \frac{K}{2R+1} \sum_{j=-R}^{R} \sin(\theta_k - \theta_{k+j} + \alpha), \quad k = \ldots, -1, 0, 1, \ldots. \tag{1}$$

with phases $\theta_k \in [0, 2\pi)$. The parameters $K \in \mathbb{R}$ and $\alpha \in (-\pi/2, \pi/2)$ are coupling strength and phase lag, respectively. The natural frequencies ω_k are randomly and independently drawn from the Lorentzian distribution

$$g(\omega) := \frac{1}{\pi} \frac{1}{1 + \omega^2} \tag{2}$$

and $R \in \mathbb{Z}^+$ is the number of neighboring oscillators, on each side, to which each oscillator is coupled. Without loss of generality, we have chosen the frequency distribution to have zero mean and unit width, which can be achieved by moving to a co-rotating frame and rescaling the coupling strength K. For numerical simulations, we will later take a finite number $k = 1 \ldots, N$ and introduce periodic boundary conditions. But for theoretical considerations, it is more convenient to choose an infinite chain with $k \in \mathbb{Z}$.

The remainder of this paper is organized as follows. In Sec. II we derive a continuum limit of our model, provide explicit expressions for the twisted states, and analyze their stability. In Sec. III we compare simulations of the finite system (1) with our results for the continuum limit. We conclude in Sec. IV with a summary and discussion of generalizations of our results.

II. CONTINUUM LIMIT ANALYSIS

As a crucial tool for our analysis we use the ansatz of Ott and Antonsen [17, 18]. In its general form, it is applicable to the continuum limit of networks of nonidentical, sinusoidally-coupled phase oscillators and allows one to study most of the interesting phenomena in a substantially simplified setting. We start by rewriting Eq. (1) in the local form

$$\frac{d\theta_k}{dt} = \omega_k + \text{Im}[Z_k(t)e^{-i\theta_k}],$$

such that oscillator k is driven by $Z_k(t) \in \mathbb{C}$, which involves an average over oscillator k's $2R + 1$ nearest neighbors:

$$Z_k(t) = \frac{K}{2R+1} \sum_{j=-R}^{R} e^{i\theta_{k+j}(t)} e^{-i\alpha}.$$

We pass now to a continuum limit, i.e. we introduce a continuous spatial variable x. The limit we choose is specified by assuming the coupling range is a macroscopic quantity, which on an unbounded domain $x \in \mathbb{R}$ can be scaled to one. To this end, we assign uniformly distributed positions

$$x_k = hk = \frac{k}{2R}$$

to the oscillators and consider the formal limit $h \to 0$, requiring at the same time that hR remains constant. The macroscopic distribution of the oscillator phases is then described by a probability density function $f(\theta, \omega, x, t)$, where x and ω are continuous variables. For a given time moment t, $f(\theta, \omega, x, t)d\theta d\omega dx$ provides the probability that an oscillator with a position in $[x, x + dx]$ and natural frequency in $[\omega, \omega + d\omega]$ has its phase in $[\theta, \theta + d\theta]$. Consequently, the spatially continuous analog of the averaged field Z_k is given by

$$Z(x, t) = \int_{-\infty}^{\infty} KG(x - y) \int_{-\infty}^{\infty} \int_0^{2\pi} f(\theta, \omega, y, t)e^{i\theta} e^{-i\alpha} d\theta \, d\omega \, dy,$$

where

$$G(s) = \begin{cases} 1/2 & \text{for} \quad |s| \leq 1, \\ 0 & \text{for} \quad |s| > 1. \end{cases} \tag{3}$$

The evolution of the function f is then given by the continuity equation

$$\frac{\partial f}{\partial t} + \frac{\partial}{\partial \theta} (fJ[f]) = 0, \tag{4}$$

where

$$J[f] = \omega + \mathrm{Im}\left[e^{-i(\theta+\alpha)} \int_{-\infty}^{\infty} KG(x-y) \int_{-\infty}^{\infty} \int_{0}^{2\pi} f(\theta',\omega,y,t)e^{i\theta'} d\theta' \, d\omega \, dy \right]. \tag{5}$$

For the nonlocal coupling used in Eq. (1) we have to use the function $G(s)$ given by formula (3). However, the analysis presented below remains valid for arbitrary even, absolutely integrable functions $G(s)$.

Following the Ott-Antonsen method [17, 18] we seek solutions of Eqns. (4) and (5) in the form

$$f(\theta,\omega,x,t) = \frac{g(\omega)}{2\pi}\left[1 + \sum_{n=1}^{\infty} \overline{z}^n(\omega,x,t)e^{in\theta} + \text{c.c.} \right], \tag{6}$$

where $\overline{z}$ denotes the complex conjugate of z and "c.c." stands for the complex conjugate of the preceding term. It is straightforward to verify that ansatz (6) solves Eqns. (4) and (5) provided $|z| \le 1$ and

$$\frac{dz}{dt} = i\omega z(\omega,x,t) + \frac{1}{2}Z(x,t) - \frac{1}{2}z^2(\omega,x,t)\overline{Z}(x,t). \tag{7}$$

Since the natural frequencies are distributed according to the Lorentzian (2), one can derive

$$\int_{-\infty}^{\infty} \int_{0}^{2\pi} f(\theta,\omega,x,t)e^{i\theta} d\theta \, d\omega = z(i,x,t),$$

using complex integration based on the analytic continuation of z; for details see [17]. Denoting now $z(i,x,t)$ by $u(x,t)$, Eq. (7) is replaced by the simpler equation

$$\frac{du}{dt} = -u(x,t) + \frac{K}{2}e^{-i\alpha}\mathcal{G}u - \frac{K}{2}e^{i\alpha}u^2(x,t)\mathcal{G}\overline{u}, \tag{8}$$

where for any locally integrable function v we define

$$(\mathcal{G}v)(x) = \int_{-\infty}^{\infty} G(x-y)v(y)dy. \tag{9}$$

Note that equations equivalent to (8)-(9) were first presented in [8], although in the context of analyzing chimera states.

A.   Uniform incoherence

The uniformly incoherent state $u(x,t) = 0$ is clearly always a solution of (8). To study its stability, we linearize Eq. (8) around this state and obtain

$$\frac{dv}{dt} = -v(x,t) + \frac{K}{2}e^{-i\alpha}\mathcal{G}v.$$

Substituting

$$v(x,t) = v_0 e^{i\kappa x}e^{\lambda t},$$

we find the spectral equation

$$\lambda = -1 + \frac{1}{2}e^{-i\alpha}K\hat{G}(\kappa), \tag{10}$$

where

$$\hat{G}(\kappa) \equiv \int_{-\infty}^{\infty} G(s)e^{-i\kappa s}ds = \int_{-\infty}^{\infty} G(s)\cos(\kappa s)ds$$

is the Fourier transform of the coupling function, G. In particular, for the coupling function (3) we obtain

$$\hat{G}(\kappa) = \frac{\sin(\kappa)}{\kappa}. \tag{11}$$

Fig. 1 shows the graph of $\mathrm{Re}(\lambda)$ vs. κ for four different values of K and $\alpha = 0$. By inserting $\mathrm{Re}(\lambda) = 0$ into (10), we obtain the stability boundary of this state in the parameter plane spanned by K and κ, for a given value of α. This stability boundary is shown as the red dashed curves in Fig. 2. Note that for $|\alpha| < \pi/2$ and small $|K|$ the uniform incoherent state is stable with respect to perturbations with all wave numbers. For positive K, it loses its stability in a long wave instability ($\kappa = 0$) at

$$K = \frac{2}{\cos\alpha},$$

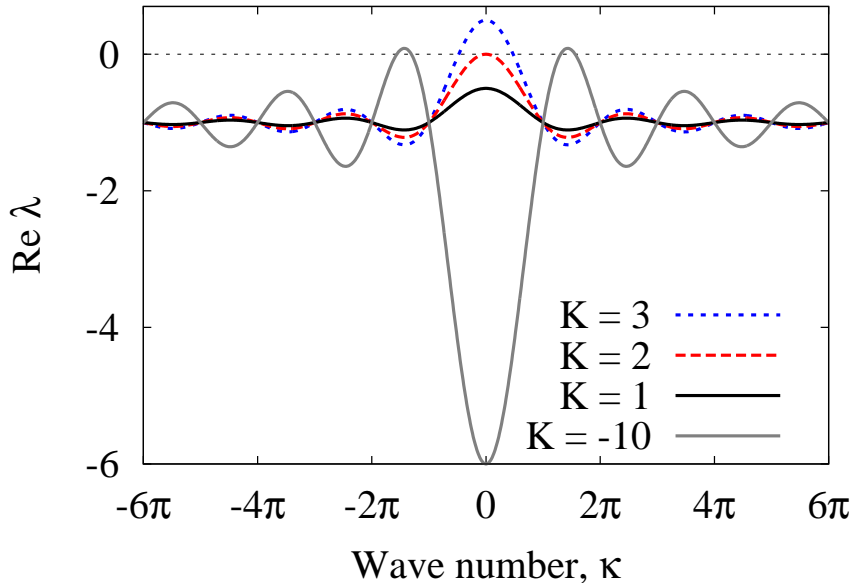whereas for negative K the instability occurs at a finite wavelength.

FIG. 1: (Color online) Spectral curves of the uniformly incoherent state, as determined by Eq. (10), for $\alpha = 0$ and coupling function (3). There is a long wave instability for increasing coupling strength K, and a finite wavelength instability for decreasing negative K.

B. Twisted states: existence

The main focus of our interest is partially coherent twisted states appearing after the destabilization of the completely incoherent state. In the continuum limit, they can be found explicitly in the form

$$u(x,t) = ae^{i(\kappa x + \nu t)}, \tag{12}$$

where κ, ν and $a > 0$ are real numbers. Substituting (12) into Eq. (8) we find

$$i\nu = -1 + \frac{K}{2}\left(e^{-i\alpha}\hat{G}(\kappa) - a^2 e^{i\alpha}\hat{G}(-\kappa)\right) = -1 + \frac{K}{2}(e^{-i\alpha} - a^2 e^{i\alpha})\hat{G}(\kappa), \tag{13}$$

where we used the identity

$$\int_{-\infty}^{\infty} G(x-y)e^{i\kappa y}dy = \hat{G}(\kappa)e^{i\kappa x},$$

and the fact that $\hat{G}(-\kappa) = \hat{G}(\kappa)$ for an even coupling function $G(s)$. Now, equating real and imaginary parts of Eq. (13) we obtain

$$a^2 = 1 - \frac{2}{K\hat{G}(\kappa)\cos\alpha} \tag{14}$$

and

$$\nu = -\frac{K}{2}(1 + a^2)\hat{G}(\kappa)\sin\alpha = \tan\alpha - K\hat{G}(\kappa)\sin\alpha. \tag{15}$$

It is easy to see that Eq. (14) has a solution with a given κ iff

$$1 - \frac{2}{K\hat{G}(\kappa)\cos\alpha} > 0. \tag{16}$$

This inequality is satisfied inside the regions bounded by the red dashed curves $K = K_c(\kappa) := 2/(\hat{G}(\kappa)\cos\alpha)$ in Fig. 2. Thus, twisted states are created as the uniformly incoherent state destabilizes.
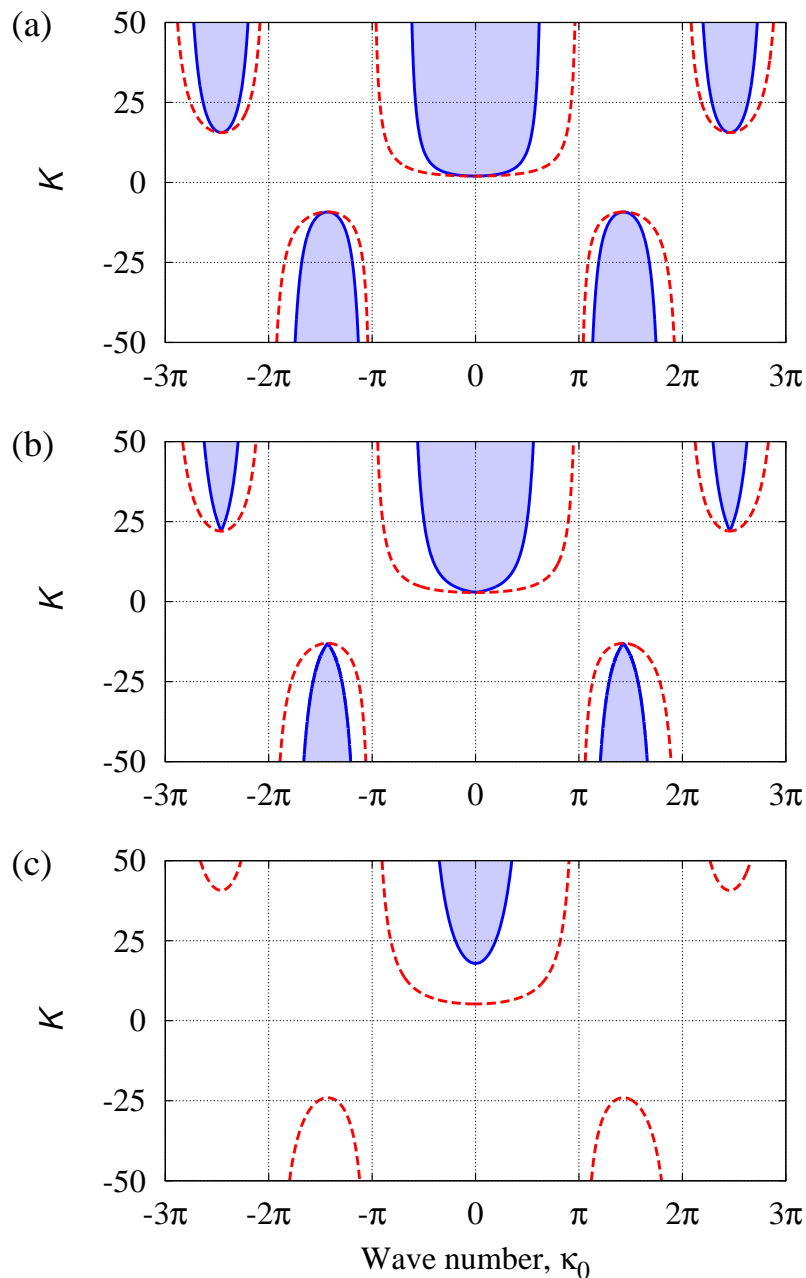
FIG. 2: (Color online) Dashed curves show the existence boundaries for twisted states, which are also the instability boundaries for the uniformly incoherent state. Solid curves mark instabilities of twisted states. Stable twisted states can be found for parameters picked from shaded regions. For increasing α, twisted states are less stable, compare (a) $\alpha = 0$, (b) $\alpha = \pi/4$, and (c) $\alpha = 3\pi/8$.

Substituting (12) into (6), evaluating the infinite series, and marginalizing over ω we obtain the probability density function

$$F(\theta, x, t) \equiv \int_{-\infty}^{\infty} f(\theta, \omega, x, t) \, d\omega = \frac{1 - a^2}{2\pi\{1 - 2a\cos[\theta - (\kappa x + \nu t)] + a^2\}}.$$

For fixed x and t, this is a unimodal function of θ, with maximum at $\theta = \kappa x + \nu t$, and width determined by a. As $a \to 0$, the distribution becomes uniform, whereas for $a \to 1$, the distribution tends to $\delta(\theta - (\kappa x + \nu t))$ [14]. From (14), we see that this case corresponds to $K \to \infty$ and we obtain the completely coherent twisted states studied in [27] for the system with identical frequencies. Accordingly, the twist is given by spatial wave number κ, both for partially and completely coherent states.

C. Stability of twisted states

Let us now consider the stability of a twisted state with a given wave number κ_0 and corresponding temporal frequency ν_0, as determined by Eq. (15). It is convenient to transform Eq. (8) into co-rotating coordinates

$$u(x,t) \mapsto U(x,t), \quad \text{where} \quad u(x,t) = U(x,t)e^{i(\kappa_0 x + \nu_0 t)}.$$

After this transformation we obtain

$$\frac{dU}{dt} = -(1 + i\nu_0)U(x,t) + \frac{K}{2}e^{-i\alpha} \int_{-\infty}^{\infty} G(x-y)e^{-i\kappa_0(x-y)}U(y,t)dy$$

$$- \frac{K}{2}e^{i\alpha}U^2(x,t)\int_{-\infty}^{\infty} G(x-y)e^{i\kappa_0(x-y)}\overline{U}(y,t)dy.$$

Substituting

$$U(x,t) = a(\kappa_0) + v(x,t),$$

where $a(\kappa_0)$ is given by Eq. (14) with $\kappa = \kappa_0$, and linearizing the result with respect to small perturbations v we arrive at

$$\frac{dv}{dt} = -\eta(\kappa_0)v(x,t) + \frac{K}{2}e^{-i\alpha} \int_{-\infty}^{\infty} G(x-y)e^{-i\kappa_0(x-y)}v(y,t)dy$$

$$- \frac{K}{2}a^2(\kappa_0)e^{i\alpha} \int_{-\infty}^{\infty} G(x-y)e^{i\kappa_0(x-y)}\overline{v}(y,t)dy \qquad (17)$$

where

$$\eta(\kappa) := 1 + i\nu(\kappa) + Ke^{i\alpha}a^2(\kappa)\hat{G}(-\kappa) = \frac{K}{2}(e^{-i\alpha} + a^2(\kappa)e^{i\alpha})\hat{G}(\kappa).$$

Introducing the vector function

$$V(x,t) = \begin{pmatrix} \operatorname{Re} v(x,t) \\ \operatorname{Im} v(x,t) \end{pmatrix}$$

and separating real and imaginary parts of (17) we rewrite this equation as follows

$$\frac{dV}{dt} = -MV(x,t) + \frac{K}{2}Q^T \int_{-\infty}^{\infty} G(x-y)\begin{pmatrix} \cos\kappa_0(x-y) & \sin\kappa_0(x-y) \\ -\sin\kappa_0(x-y) & \cos\kappa_0(x-y) \end{pmatrix} V(y,t)dy$$

$$- \frac{K}{2}a^2(\kappa_0)Q \int_{-\infty}^{\infty} G(x-y)\begin{pmatrix} \cos\kappa_0(x-y) & \sin\kappa_0(x-y) \\ \sin\kappa_0(x-y) & -\cos\kappa_0(x-y) \end{pmatrix} V(y,t)dy, \qquad (18)$$

where

$$M = \begin{pmatrix} \operatorname{Re}\eta(\kappa_0) & -\operatorname{Im}\eta(\kappa_0) \\ \operatorname{Im}\eta(\kappa_0) & \operatorname{Re}\eta(\kappa_0) \end{pmatrix} \quad \text{and} \quad Q = \begin{pmatrix} \cos\alpha & -\sin\alpha \\ \sin\alpha & \cos\alpha \end{pmatrix}.$$

Next we look for solutions to Eq. (18) of the form

$$V = V_0 e^{i\kappa x}e^{\lambda t}, \quad \text{where} \quad V_0 \in \mathbb{C}^2. \qquad (19)$$

Substituting this into Eq. (18) and using the identities

$$\int_{-\infty}^{\infty} G(x-y)\cos\kappa_0(x-y)\,e^{i\kappa y}dy = \frac{1}{2}\left(\hat{G}(\kappa + \kappa_0) + \hat{G}(\kappa - \kappa_0)\right)e^{i\kappa x},$$
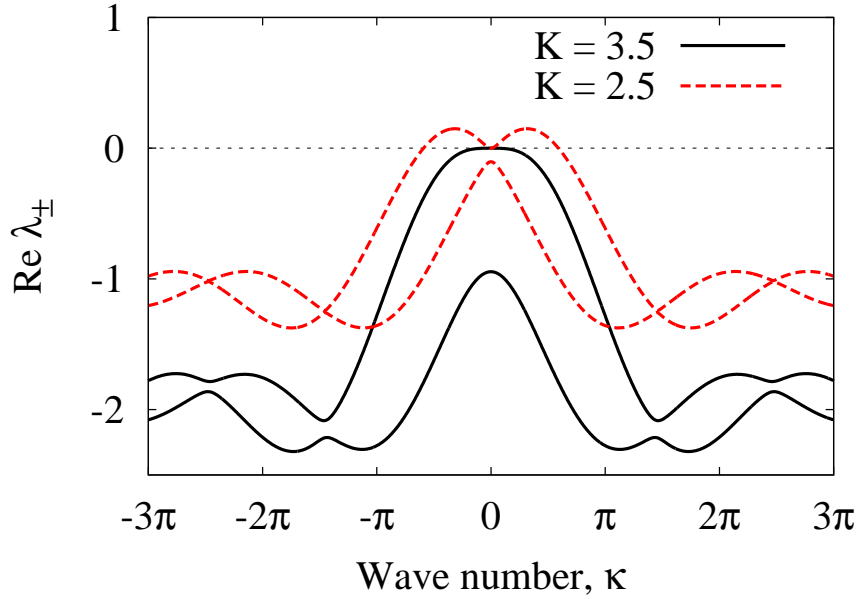
$$\int_{-\infty}^{\infty} G(x-y)\sin\kappa_0(x-y)\,e^{i\kappa y}dy = \frac{i}{2}\left(\hat{G}(\kappa + \kappa_0) - \hat{G}(\kappa - \kappa_0)\right)e^{i\kappa x},$$

FIG. 3: (Color online) Spectral curves (upper curve corresponding to λ_+, lower curve to λ_-) for the twisted state with $\kappa_0 = 1$, indicating instability (red dashed curves) for $K < K_E(\kappa_0)$ and stability (black solid curves) for $K > K_E(\kappa_0)$; ($\alpha = 0$).

we obtain the spectral equation

$$\det(\lambda I - B) = 0, \tag{20}$$

where

$$B := -M + \frac{K}{4} Q^T \begin{pmatrix} h_+(\kappa, \kappa_0) & ih_-(\kappa, \kappa_0) \\ -ih_-(\kappa, \kappa_0) & h_+(\kappa, \kappa_0) \end{pmatrix}$$

$$- \frac{K}{4} a^2(\kappa_0) Q \begin{pmatrix} h_+(\kappa, \kappa_0) & ih_-(\kappa, \kappa_0) \\ ih_-(\kappa, \kappa_0) & -h_+(\kappa, \kappa_0) \end{pmatrix}$$

and

$$h_+(\kappa, \kappa_0) := \hat{G}(\kappa + \kappa_0) + \hat{G}(\kappa - \kappa_0), \quad h_-(\kappa, \kappa_0) := \hat{G}(\kappa + \kappa_0) - \hat{G}(\kappa - \kappa_0).$$

Eq. (20) ensures the existence of non-trivial solutions of (18) of the form (19). It can be solved explicitly:

$$\lambda_\pm(\kappa) = \frac{1}{2} \left(\operatorname{tr} B \pm \sqrt{(\operatorname{tr} B)^2 - 4 \det B} \right). \tag{21}$$

Fig. 3 shows the dispersion relations Re $(\lambda_\pm(\kappa))$ for a state with twist $\kappa_0 = 1$, again using the coupling function (3). Note that according to (16), we should choose $K \geq K_c(\kappa_0)$ in order to ensure the existence of the twisted state. We observe that the twisted state with $\kappa_0 = 1$ bifurcates unstably from the completely incoherent state and eventually stabilizes for sufficiently large coupling strength K. The stability threshold can be determined by

$$\text{Re} \left(\lambda_+''(0) \right) = 0,$$

using the second derivative of $\lambda_+(\kappa)$ with respect to its argument κ that indicates where the dispersion curve (21) changes from negative to positive curvature at $\kappa = 0$. Note that one can easily check that

$$\text{Re} \left(\lambda_+(0) \right) = \text{Re} \left(\lambda_+'(0) \right) = 0$$

holds true in general. Applying this bifurcation criterion, we calculated stability boundaries of twisted states for the coupling (3), see blue lines in Fig. 2. For $\alpha = 0$, the synchronization transition at $K = 2$, where the

uniform completely incoherent state loses stability and spatially periodic patterns with different wave numbers arise, resembles the well-known Eckhaus scenario [5]. Only for the central wavelength $\kappa_0 = 0$ do we observe a direct transition from stable incoherence to a stable partially coherent state. All states with twist $\kappa_0 \neq 0$ are unstable upon creation at $K_c(\kappa_0)$ and stabilize only for some $K_E(\kappa_0) > K_c(\kappa_0)$ where their amplitude is already different from zero. Note that the curves for existence (red dashed curves in Fig. 2) and stability (blue solid curves in Fig. 2) coincide with the classical Eckhaus parabolas only to leading order in the vicinity of the central wavelength $\kappa_0 = 0$. Their asymptotic wave numbers for $K \to \infty$ coincide, for $\alpha = 0$, with the corresponding values calculated in [27] for the case of identical frequencies. For $\alpha > 0$, the temporal frequency of the bifurcating twisted waves is different from zero, the critical coupling $K_c(0)$ for the onset of partial coherence increases, and the stability region becomes slightly smaller. But there are no qualitative changes until $\alpha = \pi/4$ where the stability curve detaches from the existence curve and new stable regimes beyond partially coherent twisted states appear.

III. FINITE-N SIMULATIONS

In this section we compare the theoretical predictions of the continuum limit analysis with numerical results for the finite system obtained by introducing periodic boundary conditions to the discrete oscillator chain (1). Correspondingly, we have to restrict to solutions of the continuum limit that respect periodic boundary conditions on a finite interval $[0, L]$. The main consequence for our analysis is that possible twisted states and their unstable modes also have to satisfy this periodicity condition and appear for a discrete sequence of wave numbers $\kappa = 2\pi q/L$, $q \in \mathbb{Z}$, only. However, for sufficiently large L there are no substantial differences, c.f. [26]. For a proper correspondence to the continuum limit, the total number of oscillators N and the discrete coupling range R have to satisfy $N = LR$. For fixed N and identical frequencies system (1) has N different uniformly twisted states [6], parametrized by the integer $q \in \{0, 1, 2, \ldots, N - 1\}$, described by

$$\theta_k = \frac{2\pi}{N} q k, \quad k = 1, 2, \ldots, N. \tag{22}$$

These states can be identified with their continuum limit counterparts

$$u(x, t) = e^{i\kappa x}, \quad \text{where} \quad \kappa = 2\pi q/L. \tag{23}$$

Recall that for non-identical oscillators we obtained partially synchronized twisted states described with a more general ansatz (12).

Using exact twisted states (22) with $q = 0, \pm 1, \pm 2$ as initial data, we performed numerical simulations of system (1) with $N = 1000$, $R = 100$, $\alpha = 0$ and $K = 10$. Discarding transient dynamics of 100 time units, we recorded typical final snapshots as shown in Fig. 4. Each of these snapshots appears as a swarm of points distributed around a central curve that is close to an exact twisted state. However, decreasing the coupling radius to $R = 50$ we observe already a strong influence of the finite size fluctuations induced by the realization of the randomly distributed frequencies. We obtain the significantly distorted twisted states shown in Fig. 5. Their central curves are bent and deviate significantly from exact twisted states. Despite this fact, statistical properties of these distorted twisted states are well described by the continuum limit. In order to see this, for each snapshot in Fig. 5 we calculated the approximate local mean field

$$w_k = \frac{1}{2R + 1} \sum_{j=-R}^{R} e^{i\theta_{k+j}}. \tag{24}$$

The argument of w_k, $\arg(w_k)$, resembles the central curve of the oscillators (green lines in Fig. 5), which allows us to determine the twists q of these distorted states as a topological invariant. Next, we consider the absolute value, $|w_k|$, which displays irregular oscillations around some constant level W, where

$$W = \frac{1}{N} \sum_{k=1}^{N} |w_k|. \tag{25}$$

Taking into account that in the continuum limit, the quantity analogous to w_k is given for a twisted state (12) by the formula

$$w(x, t) = \frac{1}{2} \int_{-1}^{1} a e^{i(\kappa x + \kappa y + \nu t)} dy = a\hat{G}(\kappa) e^{i(\kappa x + \nu t)},$$

we can compare the amplitude $|a\hat{G}(\kappa)|$ with its finite dimensional counterpart W. Fig. 6 shows for $N = 1000$ good coincidence of these values for the non-twisted state. (A comparison for twisted states is shown below.)
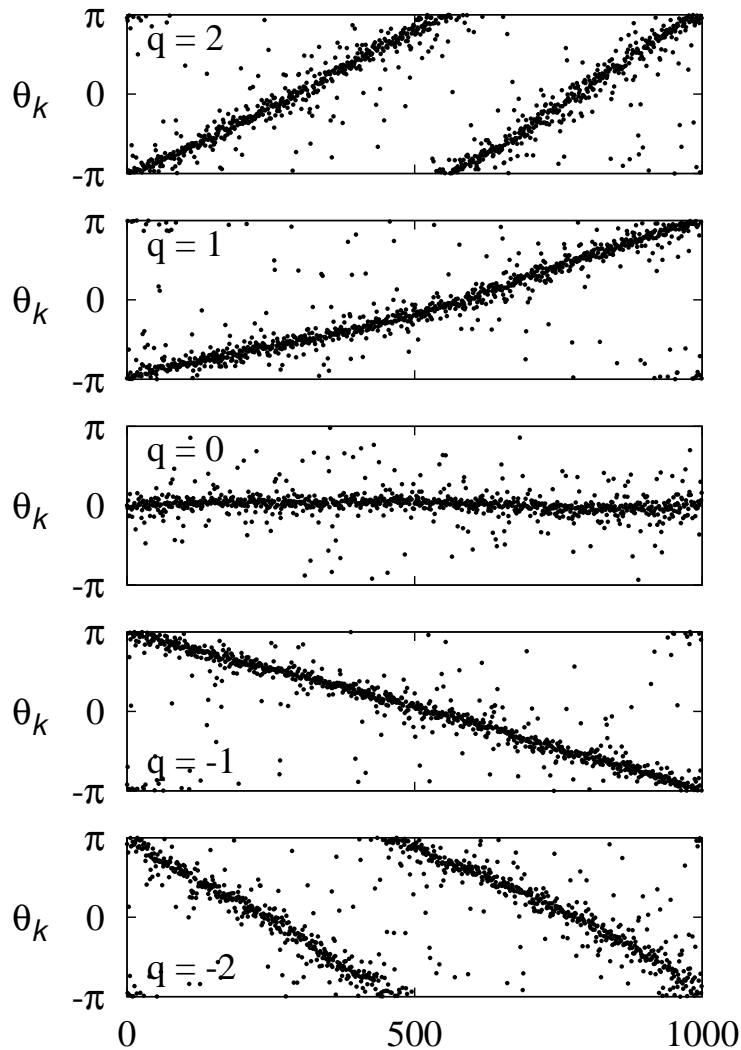
FIG. 4: Partially synchronized twisted states observed in system (1) with $N = 1000$, $R = 100$, $\alpha = 0$ and $K = 10$.

In order to verify the Eckhaus stability boundaries, we performed another series of numerical simulations. It is natural to assume that an exact q-twisted state used as initial data for system (1) will typically be attracted to the corresponding partially synchronized q-twisted state, provided the latter is stable. We checked this hypothesis numerically as follows. Using an exact q-twisted state as initial data, we performed 1000 simulations of system (1), each with a different realization of the frequencies ω_k, and estimated the probability of being attracted to a stable partially synchronized state with the same twist, see Fig. 7. We observed that as we vary the wave number $\kappa = 2\pi q R/N$ the probability tends to vanish close to the Eckhaus instability boundary.

For fixed parameters, a large number of different stable twisted states may coexist, and the size of their basins is an important issue [13]. Indeed, in [27] it was pointed out that for identical oscillators, depending on the twist, there is a remarkable difference in the sizes of their basins. In a similar way as in [27] we investigated the statistical properties of the basin sizes. For fixed N, R, α and K we performed 10000 numerical simulations with different realizations of natural frequencies ω_k and random uniformly distributed initial data. For each simulation, we take its final snapshot after 100 time units to allow for transients to die away, and extract its topological twist q. Collecting 10000 samples we construct a probability distribution histogram with respect to the twist q. The obtained results are shown in Fig. 8. Similar to the results of Wiley et al. [27], we observe that the distribution of basin sizes becomes Gaussian as N increases. Moreover, the standard deviation of the distribution depends on the ratio $r = R/N$ rather than on R and N separately.

Fig. 9 shows the dependence of the Gaussian's width, σ, as r and K are varied. We see that $1/\sigma^2$ seems to be proportional to r (compare with Fig. 3 in [27]). On the other hand, there seems to be a monotonic growth of σ with increasing coupling strength K that saturates as $K \to \infty$ at the corresponding value for identical oscillators.
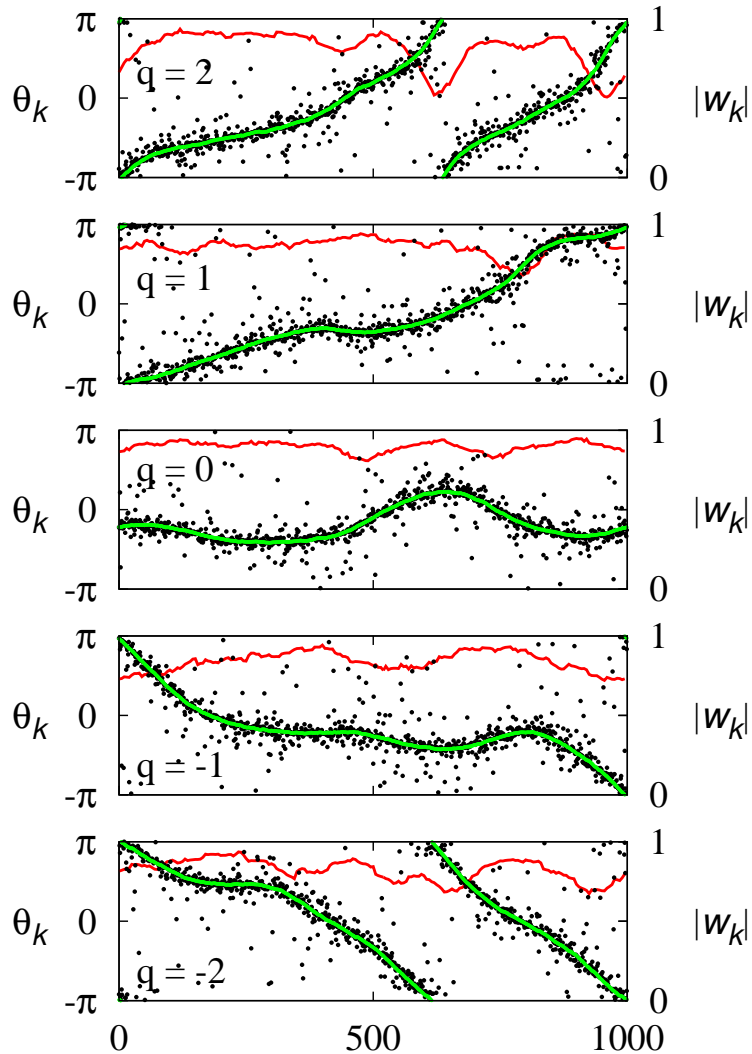
FIG. 5: (Color online) Partially synchronized twisted states observed in system (1) with $N = 1000$, $R = 50$, $\alpha = 0$ and $K = 10$. Red and green solid lines show $|w_k|$ and $\arg(w_k)$ calculated by (24).

IV. CONCLUSION AND DISCUSSION

We have considered twisted waves in arrays of nonlocally coupled non-identical phase oscillators. By passing to the continuum limit and using the Ott/Antonsen ansatz we have derived a nonlocally coupled differential equation governing the evolution of a complex-valued spatially-dependent order parameter. For twisted states, the magnitude of this quantity indicates the level of synchrony of nearby oscillators, while its argument can be used to define the twist of the corresponding state. We explicitly found twisted states in the continuum limit and showed that their stability can also be calculated explicitly. There is a strong analogy between the appearance of twisted states and their subsequent stabilization as the coupling strength is increased, and the Eckhaus instability [26, 28]. Finite-N simulations were performed which showed that once finite-size effects are taken into account, the results from the analysis of the continuum system correctly describe the dynamics of a finite network.

The main work with which we should compare our results is that of Wiley et al. [27]. We used nonidentical oscillators, while they used identical ones. This leads to several complications. For their system, all twisted states always exist for non-zero coupling strength. When using nonidentical oscillators, there is competition between the tendency for oscillators to move at their own intrinsic speed and the coupling term, which acts to synchronize the oscillators, as in the original Kuramoto system [2, 24]. We thus have a more complicated situation, where the existence of twisted states depends not only on the strength of coupling, but the value of the twist (see Fig. 2). Our continuum limit equations [(8) and (9)] are for a complex variable with both phase and magnitude, whereas Wiley et al. have an equation for a purely angular variable. This results in
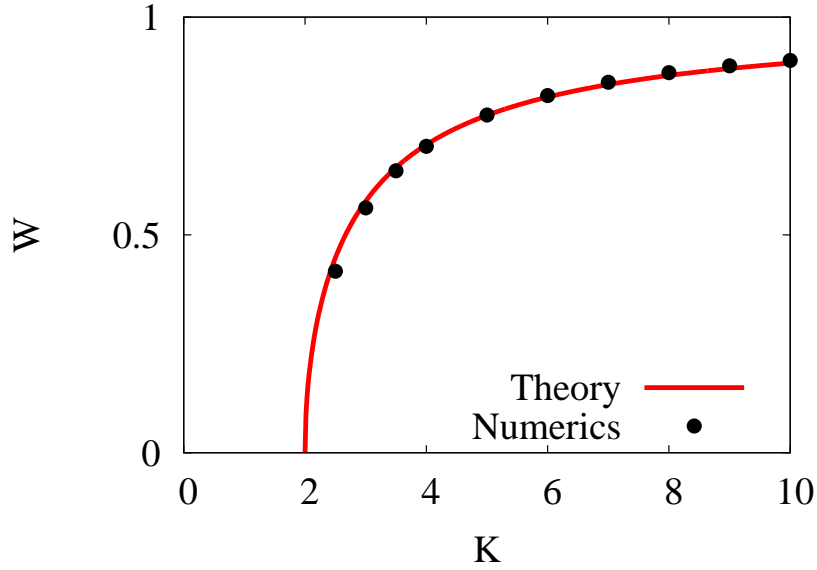
FIG. 6: (Color online) Averaged local mean field W of the non-twisted partially synchronized state ($q = 0$). Theoretical values calculated by formula (14) (solid line) and numerical data (dots) obtained by the application of formula (25) to non-twisted final states of system (1) with $N = 1000$, $R = 100$ and $\alpha = 0$.
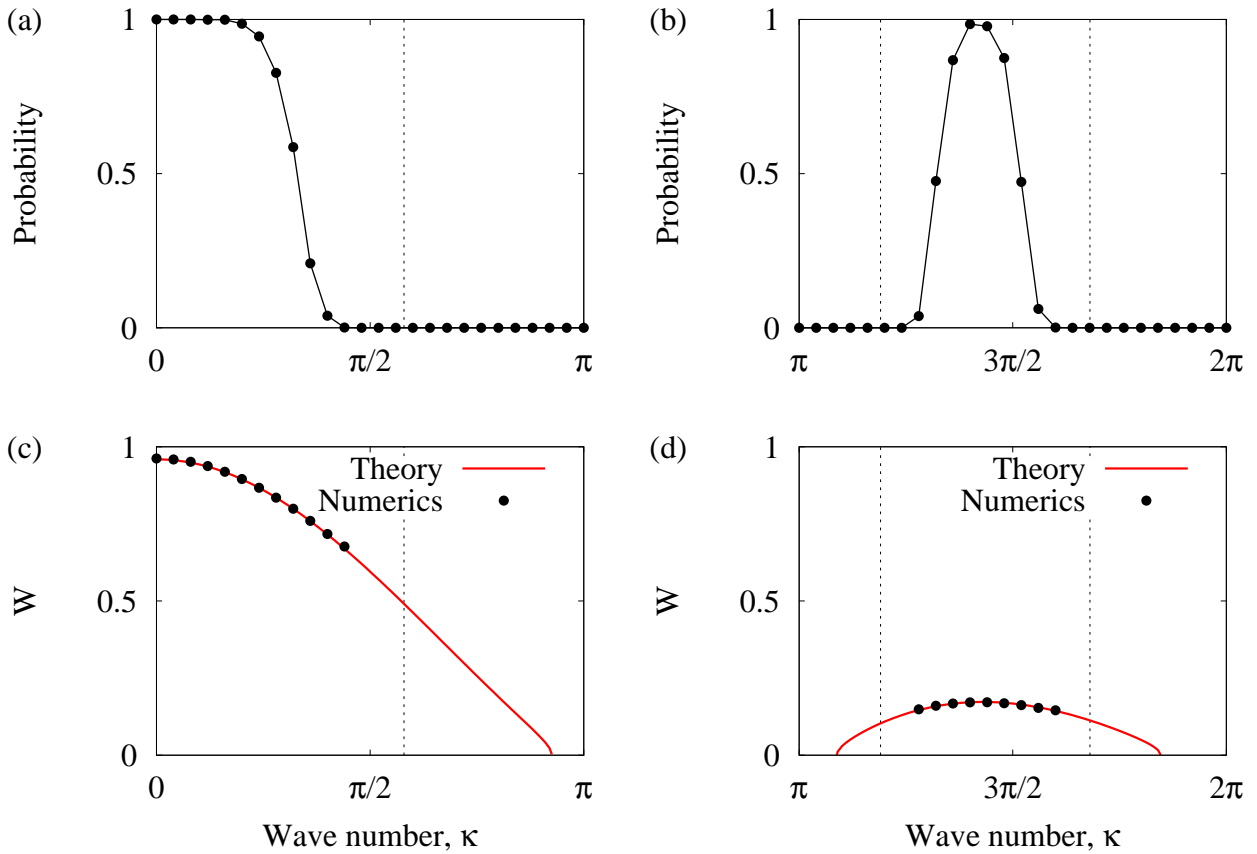

FIG. 7: (Color online) Top: Probability of obtaining partially synchronized twisted states starting from the corresponding exact twisted state for $K = 25$ (a) and $K = -25$ (b). Other parameters: $N = 5000$, $R = 100$, $\alpha = 0$. Eckhaus stability boundaries are shown as dashed vertical lines (see Fig. 2(a)). The lower two panels show the averaged local mean field W given by (25) for these partially-synchronized states (points) and the theoretically predicted value given by formula $|a\hat{G}(\kappa)|$ with (14) and (11) (solid line).
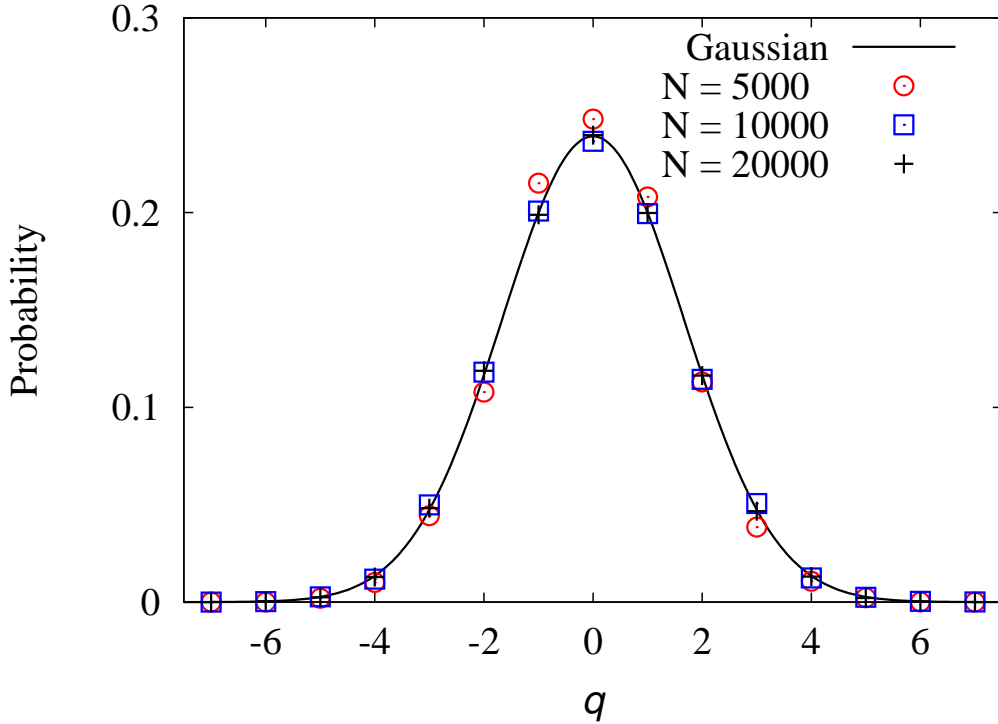
FIG. 8: (Color online) Distribution of basin sizes for the various partially synchronized twisted states. The data points were obtained from 10000 simulations of system (1) with random initial data and independent realizations of natural frequencies ω_k. Parameters: $R/N = 0.01$, $K = 10$ and $\alpha = 0$. Solid line shows a Gaussian fit of points with $N = 20000$.
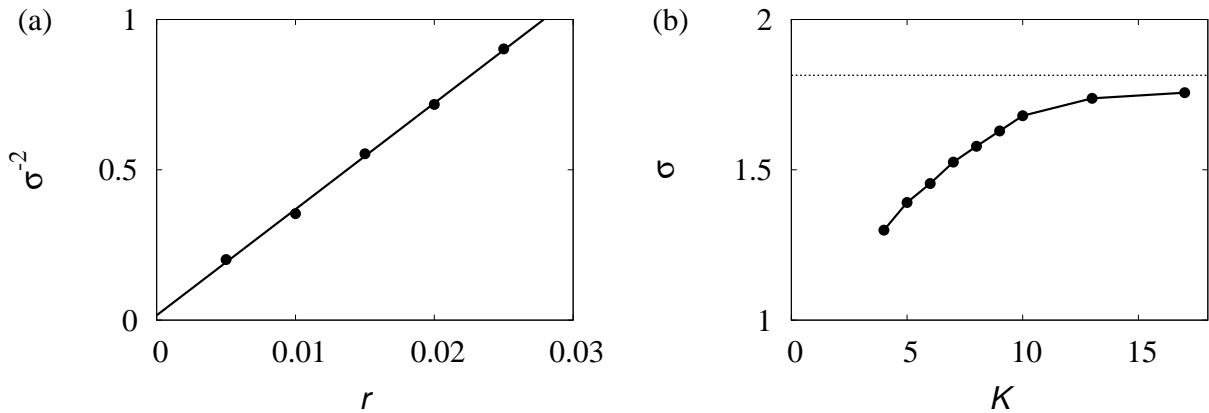

FIG. 9: (a) Inverse of the variance of the probability distribution histogram, σ^{-2}, versus ratio $r = R/N$, for fixed $K = 10$. (b) Width of distribution, σ, as a function of coupling strength K, for fixed $r = R/N = 0.01$. For increasing coupling strength K, the distribution becomes broader and its width saturates (dotted line) for $K \to \infty$. Parameters: $N = 10000$, $\alpha = 0$.

the stability calculations shown here being more involved than those of Wiley et al. These authors found that stability depended only on the width of the coupling kernel (r) and the twist of a state, whereas in our model the strength of coupling (K) also plays a role (again, see Fig. 2). Our work can be seen as a direct extension of the work of Wiley et al., and setting $a = 1$ and $\alpha = 0$ it can be shown that our stability results reduce to theirs. In other work, Tsimring et al. briefly considered nonidentical oscillators with nonlocal repulsive coupling [25].

Girnyk et al. [6] considered the same system as Wiley et al., but with negative (repulsive) coupling. Hence our system, with negative K, can be regarded as a generalization of theirs. As well as considering twisted states, these authors also found stable "multi-twisted" states, for which on a part of the domain the twist was approximately constant, but on the rest of the domain the twist was also approximately constant although of opposite sign. We have seen similar states in our heterogeneous network (see Fig. 10) but leave their analysis
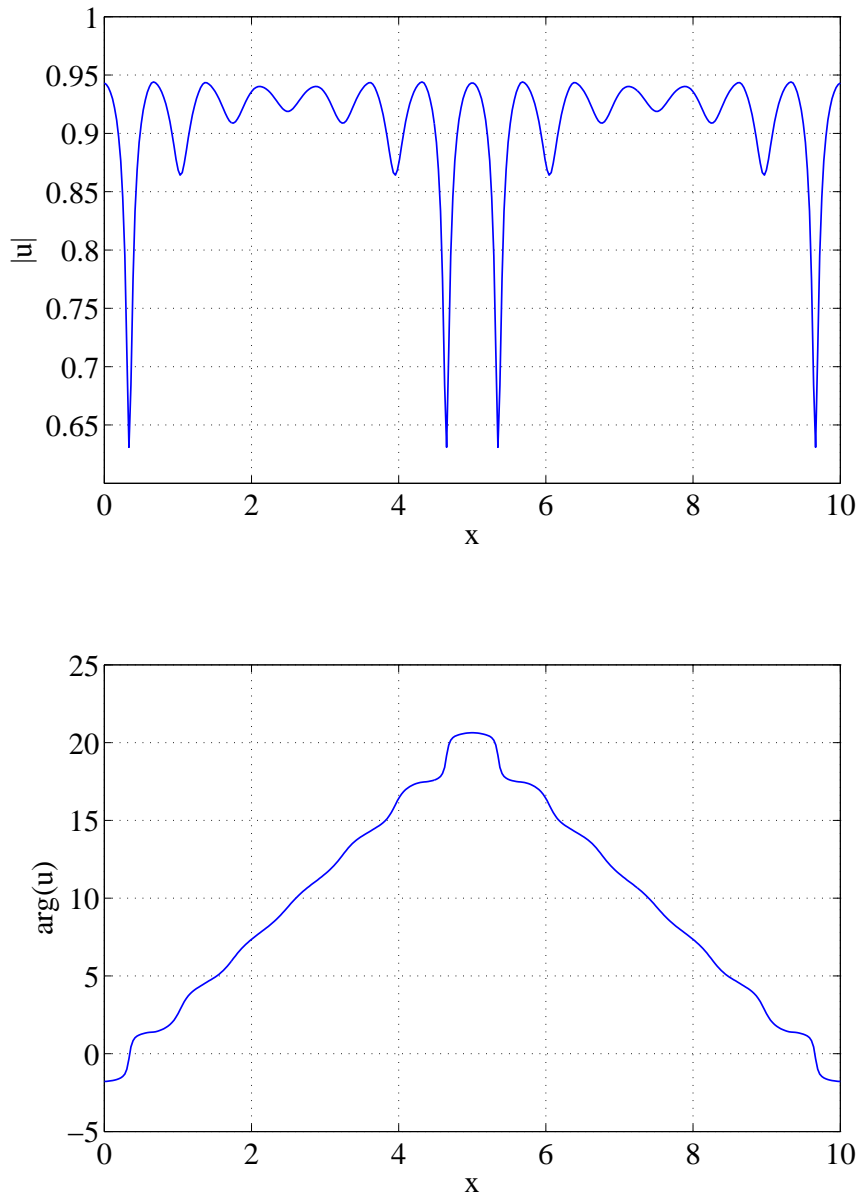
FIG. 10: (Color online) A steady-state solution of (8)-(9) showing the modulus of u (top) and its argument (bottom). This is a multi-twisted state. Parameters: $K = -70, \alpha = 0$.

for the future. Other generalizations of the work presented here could include the presence of delays, either space-dependent [21], constant [15] or distributed [9]. Another possibility is to investigate two-dimensional domains [9, 11, 16], or the use of a different coupling function.

We conclude by mentioning that we have not provided a complete description of the dynamics of (1). Looking at Fig. 2(c) we see that for $K = 7$, say, the completely incoherent state and all partially synchronized twisted states are unstable. Simulating the system for this value of K we obtain complicated spatio-temporal dynamics, as shown in Fig. 11, similar to those described for the complex Ginzburg-Landau equation [4].

[1] D. M. Abrams and S. H. Strogatz, Int. J. of Bif. and Chaos **16**, 21 (2006).
[2] J. Acebrón, L. Bonilla, C. Pérez Vicente, F. Ritort, and R. Spigler, Rev. Mod. Phys. **77**, 137 (2005).
[3] N. J. Balmforth and R. Sassi, Physica D **143**, 21 (2000).
[4] H. Chate, Nonlinearity **7**, 185 (1994).
[5] W. Eckhaus, *Studies in Nonlinear Stability Theory*, Springer, Berlin, 1965.
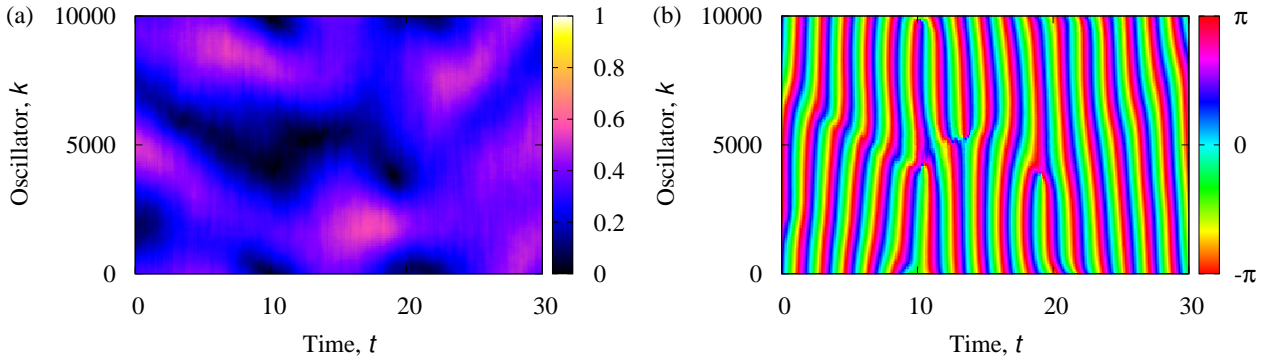[6] T. Girnyk, M. Hasler, and Y. Maistrenko, Chaos **22**, 013114 (2013).

FIG. 11: (Color online) Space-time plots of $|w_k|$ (a) and $\arg(w_k)$ (b) calculated using (24) along the trajectories observed in system (1) with $K = 7$. Other parameters: $N = 10000$, $R = 1000$, and $\alpha = 3\pi/8$. Initial data: identical phases of all oscillators.

[7] Y. Kuramoto and D. Battogtokh, Nonlinear Phenom. Complex Syst. **5**, 380 (2002).
[8] C. Laing, Physica D **238**, 1569 (2009).
[9] C. Laing, Physica D **240**, 1960 (2011).
[10] W. S. Lee, J. G. Restrepo, E. Ott, and T. M. Antonsen, Chaos, **21**, 023122 (2011).
[11] E. A. Martens, C. R. Laing and S. H. Strogatz, Phys. Rev. Lett. **104**, 044101 (2010).
[12] G. S. Medvedev, Physica D **266**, 13 (2014).
[13] P. J. Menck, J. Heitzig, N. Marwan, and J. Kurths, Nature Physics **9**, 89 (2013).
[14] O. E. Omel'chenko, Nonlinearity **26**, 2469 (2013).
[15] O. E. Omel'chenko, Y. L. Maistrenko and P. A. Tass, Phys. Rev. Lett. **100**, 044105 (2008).
[16] O. E. Omel'chenko, M. Wolfrum, S. Yanchuk, Y. L. Maistrenko, and O. Sudakov, Phys. Rev. E **85**, 036210 (2012).
[17] E. Ott and T. M. Antonsen, Chaos **18**, 037113 (2008).
[18] E. Ott and T. M. Antonsen, Chaos **19**, 023117 (2009).
[19] A. Pikovsky and M. Rosenblum, Phys. Rev. Lett. **101**, 264103 (2008).
[20] A. Pikovsky, M. Rosenblum, and J. Kurths, *Synchronization: A Universal Concept in Nonlinear Sciences*, Cambridge University Press, 2001.
[21] G. C. Sethia, A. Sen and F. M. Atay, Phys. Rev. Lett. **100**, 144102 (2008).
[22] G. C. Sethia and A. Sen, Phys. Rev. E. **81**, 056213 (2010).
[23] S. Shima and Y. Kuramoto, Phys. Rev. E **69**, 036213 (2004).
[24] S.H. Strogatz, Physica D **143**, 1 (2000).
[25] L. S. Tsimring, N. F. Rulkov, M. L. Larsen, and M. Gabbay, Phys. Rev. Lett. **95**, 014101 (2005).
[26] L. S. Tuckerman and D. Barkley, Physica D **46**, 57 (1990).
[27] D. Wiley, S. Strogatz, and M. Girvan, Chaos **16**, 015103 (2006).
[28] S. Yanchuk and M. Wolfrum, Phys. Rev. E **77**, 026212 (2008).